American Journal of Medical and Biological Research, 2017, Vol. 5, No. 2, 23-30
Available online at http://pubs.sciepub.com/ajmbr/5/2/3

DOI:10.12691/ajmbr-5-2-3

To Estimate Pulmonary Arterial Compliance and Pulse Wave Velocity in Cerebral-Cardiovascular Patients Using CT Cardiac Images

WeiChih Hu[1,*], Hsuan-Ming Tsao[2], Jian Xiang Zhi[2], Harmon Chris T. Herman[3], Lemmuel L. Tayo[3], Yashbir Singh[1], Kathiravan S[4], João Manuel R.S. Tavares[5], Chandan Chakraborty[6]

[1]Department of Biomedical Engineering, Chung Yang Christian University, Chung Li, Taiwan
[2]Divisions of Cardiology, National Yang Ming University Hospital and National Yang Ming University, Yi-Lan, Taiwan
[3]Mapua Institute of Technology, Manila, Philippines
[4]Department of Computer Science and Information Engineering, National Ilan University, Taiwan
[5]Instituto de Ciência e Inovação em Engenharia Mecânica e Engenharia Industrial, Departamento de Engenharia Mecânica, Faculdade de Engenharia, Universidade do Porto, Portugal
[6]School of Medical Science & Technology (SMST), Indian Institute of Technology Kharagpur, India
*Corresponding author: weichihhu@cycu.edu.tw

Abstract Arterial stiffness has been proven to be one of the most promising diagnostic and prognostic features of many cardiovascular diseases (CVD). Arterial compliance (AC) and pulse wave velocity (PWV) allows a good quantitative assessment of arterial stiffness. To estimate pulmonary Arterial Compliance and Pulse Wave Velocity in Cerebral-Cardiovascular Patients using 64-Row Multi-Detector Computed Tomography Cardiac Images. Here in this work, we have used an in house developed three-dimensional reconstruction algorithm that extracts high-resolution cardiac Computer Tomography images in Digital Imaging and Communications in Medicine (DICOM) format from nine subjects. The subjects consist four patients with stroke (SR) turned to atrial fibrillation (AF) and five patients with both SR and AF. The calculation showed strok volume of Left and Right Ventricles, which are near equal to 62.56±12.61 ml and 65.95±13.13 ml, respectively, with a good positive correlation ($R = 0.717$, $p < 0.0001$) while pulse wave velocity and arterial compliance are calculated to be 0.21±0.0665 m/s and 0.09 ± 0.0547 ml/mmHg for patients with SR turned AF, 0.15±0.0502 m/s and 0.10 ± 0.0438 for the SR and AF patients. We concluded that the derived methodology for calculation of PWV and AC from 3D cardiac CT images could be used as an index in the evaluation of arterial stiffness.

Keywords: *arterial compliance, arterial stiffness, Computer Tomography, Digital Imaging, Cardiac stroke*

Cite This Article: WeiChih Hu, Hsuan-Ming Tsao, Jian Xiang Zhi, Harmon Chris T. Herman, Lemmuel L. Tayo, Yashbir Singh, Kathiravan S, João Manuel R.S. Tavares, and Chandan Chakraborty, "To Estimate Pulmonary Arterial Compliance and Pulse Wave Velocity in Cerebral-Cardiovascular Patients Using CT Cardiac Images." *American Journal of Medical and Biological Research*, vol. 5, no. 2 (2017): 23-30. doi: 10.12691/ajmbr-5-2-3.

1. Introduction

The population is aging in the world at a substantial rate and old population is significantly leading to a number of deteriorations including cardiovascular diseases. It usually occurs because of the change in arterial structure and function including arterial stiffening and compliance [1,2]. Arterial stiffness is the most important factors of estimating the cardiovascular risk in various disease conditions [1]. The pulse wave velocity (PWV) and arterial compliance (AC) is a good indicator of the arterial stiffness along with atrial fibrillation (AF) [2] and stroke (SR) [3]. There are many invasive and non-invasive methods to assess the pulse wave velocity [4,5] and arterial compliance [6]. Arterial stiffness calculations can be classified into three categories the blood pressure, ultrasound Doppler and magnetic resonance (MR) techniques [1]. In a recent meta-analysis research, aortic PWV was found to improve cardiovascular ailment prediction in models that included standard risk factors (smoking, hyperglycemia, hypertension etc.), therefore it is suggested that it may prove beneficial for better identification of cardiac disease in aging high-risk population. Till now, there is no pharmacological approach which is commonly used in clinical practice to decrease arterial stiffness, thus new therapeutic approaches to decrease arterial stiffness is highly desirable (Janić, Miodrag, 2014). Recent research have shown that computed tomography (CT) imaging permits high resolution non-invasive imaging of the heart and associated arteries, i.e., coronary arteries and pulmonary artery. Computed tomography also offers very fast image-acquisition making medical diagnosis less tedious [7]. Therefore, we propose a method for calculation of the

pulmonary arterial compliance and PWV. The main objective of this work is to design a computational pipeline from high resolution cardiac CT images in DICOM (Digital Imaging and Communications in Medicine) format that can compute the total arterial and ventricular compliance of the reconstructed models.

2. Methods

2.1. Study Design

The study is divided into two parts: [8] The validation of the new non-invasive method in determining ventricular and arterial volume using a 3D reconstruction software and [1] The estimation and determination of the stroke volume of LV and RV as well as the correlation of pulse wave velocity and arterial compliance in both the right ventricle and pulmonary artery of patients with various cardiovascular disease (CVD). The study is approved by the Investigation Review Board (IRB) of National Yang-Ming University Hospital at Taipei, Taiwan.

2.2. Study Group

All computed tomography (CT) images of the subjects are provided by National Yang-Ming University Hospital in Taipei, Taiwan. Seventeen cardiac patients are involved in the study which is 42-86 year-old. There are eleven men and six women which is 42 to 86 years old. Nine patients with SR and AF while eight patients have SR turned to AF. This is an observational study. The patients with paroxysmal AF and a first episode of acute ischemic cerebral infarction admitted to neurological ward for assessment. The cause of the stroke is classified as AF-related based on the definitions of the SSS-TOAST system. All stroke patients are diagnosed an AF related stroke if it is due to AF without significant valvular disease and there is no other etiologies present. The exclusion criteria is included AF rhythm in the 48 hours after admission, serum creatinine more than 2 mg/dl, a history of contrast allergy or inability of the participant to provide informed consent.

2.3. Computed Tomography Study

Description of the adopted computed tomography protocols have been reported [9,10,11]. The Right Ventricle (RV), left ventricle (LV) and Pulmonary Arterial (PA) images are acquired by electrocardiographically gated, 64-slice multidetector computed tomography scanner (Brilliance CT 64-channel configuration, Philips Healthcare, Amsterdam, Netherlands). All participants underwent contrast-enhanced computed tomography scanning during sinus rhythm. Patients are instructed to hold their breath for acquiring the images, which covers an area from the superior margin of the pulmonary hilum to the cardiac apex (Collimation of 64 x 0.5 mm, Gantry rotation time of 350 ms, Table speed of 6.3 mm/rotation, Tube voltage of 120 kV and Effective tube current of 545 mA). Acquisition time is 8 to 12 seconds that depends on heart rate [12]. The developed computational pipeline is shown in Figure 1. The cardiac CT images are extracted from the DICOM files using image reconstruction software, developed by Department of Biomedical Engineering, Chung Yuan Christian University (Chung-Li, Taiwan). DICOM is the standard format used in medical imaging that store patient's information such as age, weight, height, Systolic Blood Pressure (SBP) and Diastolic Blood Pressure (DBP) [13]. Each scanned slice has a dimension of 512 x 512 pixels and all temporal slices are collectively obtained for each patient during one complete heartbeat cycle. As shown in Figure 2, each patient's electrocardiogram R-R Interval is divided into ten time series. Each of the time series corresponds to the various activities of the heart to one complete cardiac cycle. Each one of the ten time series is composed of 383 frames of CT gated-cardiac images which sums up to 3830 frames of data set for processing in every patient. The volume change with respect to each time series is computed, from the end-systole of the atrium that is at the beginning of the R wave (0 %) up to the end-diastole of the right ventricle at the end of the P wave (90%), in order to determine the total arterial and ventricular volumes of each patient during one complete heartbeat.

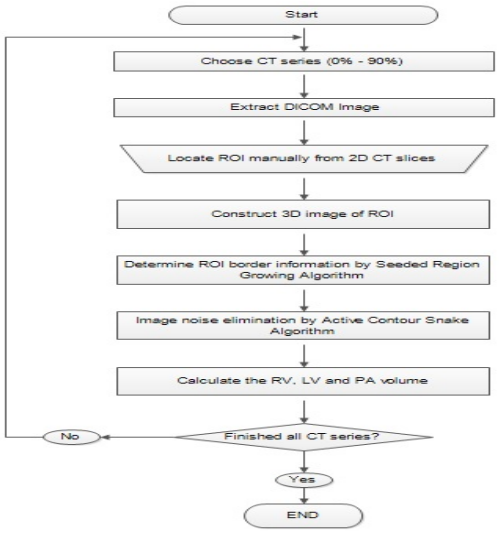

Figure 1. Developed computational pipeline for the determination of ROI volumes in CT images.

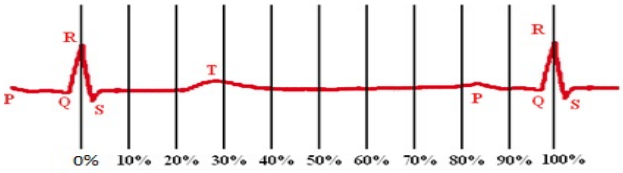

Figure 2. One electrocardiogram partitioned into ten time series.

(i) Regions of Interest

Right and Left ventricles can easily be located in the 2D CT image slices because of their large size. Here, we want to calculate the volume of the main pulmonary artery. Thus, a good resampling angle which clearly shows the location of the PA must be determined. All ROI volumes are calculated from the central axis position which clearly shows the pulmonary arterial circle and ventricular circle. However, the central axis position is determined by cutting the PA- 3D image 6 slices up and 6 slices down so as to eliminate non ROI parts, the image rebuilt with

respect to the central axis position to have a clear perspective of the ROI. The Open Graphics Library (OpenGL (version 4.3), Silicon Valley Inc.) and the Multi-platform Application Programming Interface (API) is used to reconstruct the 3D models from the cardiac CT data sets.

(ii) Seeded Region Growing Algorithm

A segmentation technique defines the borders of the anatomical structures of both the right ventricle and pulmonary artery. We applied the Seeded Region Growing Algorithm [8] Figure 3 to group parts of our CT images into units that are homogenous with respect to the image's pixel intensities. The first step in this segmentation technique is to select and label a set of seed pixels. The regions are grown starting from these seed pixels to adjacent pixels depending on their intensity.

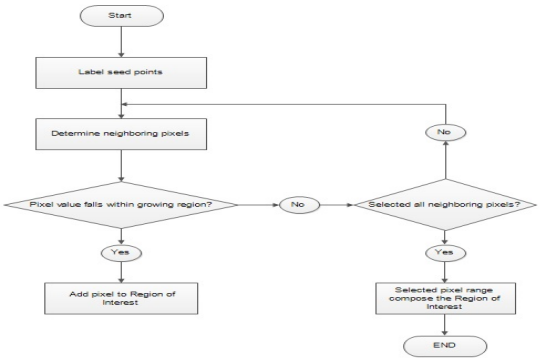

Figure 3. Seeded region growing algorithm used in the first segmentation step

(iii) Active Contour Algorithm

The limitation of the previous segmentation algorithm is its pixel location dependency. To overcome and enhance the segmentation results, we used the Active Contour Algorithm known as Snake algorithm which is developed by Kass, Witkin, and Terzopoulos in 1988 [14]. The initial edges used in the Snake Algorithm are extracted by the seeded region growing algorithm.

(iv) Volume Calculation

Modified Simpson's Rule [15] is used to quantify the volume of ventricles and pulmonary artery. This method is based on calculation of total ventricular and arterial volume from the summation of a stack of elliptical discs of CT slices. We used the snake model to identify each slice's endocardial boundary. Afterwards, the central axis position was determined in each slice by defining normal lines perpendicular to the tangent points as shown in Figure 4.

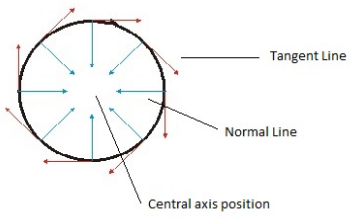

Figure 4. The central axis position is determined, in this representative slice, as the intersection of all normal lines perpendicular to the tangent points

The area under each slice's tangent line and normal line is calculated using the vector cross product formula, which is half the area of a parallelogram:

$$Area = \frac{1}{2}\left\|\vec{u}\right\|\left\|\vec{v}\right\|\sin\varnothing. \quad (4)$$

Therefore, the total area in each slice is the summation of all the areas under these vectors. Moreover, the volume of each temporal slice was computed considering a slice thickness equal to 0.9 mm and according to:

$$Volume_{slice} = Surface\ Area * Slice\ Thickness \quad (5)$$

Consequently, the total volume of the ROIs is equal to the summation of all the slice volumes as:

$$V_{ROI} = \sum_{i=1}^{n} Volume_{slice}. \quad (6)$$

(iv) Stroke Volume Calculation

We calculated the stroke volume to determine if the blood pumped from the LV is equal to the blood pumped from the RV. Its value was obtained by subtracting end-diastolic volume (40%) from end-systolic volume (0%) in both the left and the right ventricle according to:

$$SV = EDV - ESV. \quad (7)$$

Where SV is the Stroke Volume; EDV is End of the Diastolic Volume; and, ESV is the End of the Systolic Volume.

(v) Arterial Compliance and Pulse Wave Velocity Calculation

The arterial compliance of both the pulmonary artery and the right ventricle was computed from dividing the ROIs respective volumes by each patient's corresponding Right Ventricle Systolic Pressure (RVSP) as:

$$AC_{PA/RV} = \frac{V_{PA/RV}}{RVSP}. \quad (8)$$

Where V is the volume change over time; AC is representing the Arterial Compliance; PA is representing the Pulmonary Arterial; and, RV is representing the Right Ventricle. AC_{PA} is stand for the compliance of pulmonary arterial. All RVSP data is collected by echocardiography, readily provided by the National Yang-Ming University Hospital (Taipei, Taiwan) which is then included in the DICOM file. The PWV of the pulmonary artery is computed by first plotting the time intervals versus the pixel intensities for each of the temporal slice. In this study, the pulse wave consisted of 20 slices for each patient. From the pulse wave propagation plot we measured the lengths of the arterial segments (Δd) by locating and getting the difference of the steepest slope and the first slice to intersect with it. This intersection defines the starting point of the impulse. Afterwards, the differences among the slices are multiplied by the slice thickness (equal to 0.9 mm). We then used the individual heart rate of each patient to compute for the time interval (Δt) for each of the impulses:

$$PWV = \frac{\Delta d}{\Delta t}. \quad (9)$$

2.4. Statistical Analysis

All quantitative data is expressed as the mean ± standard deviation. Regression analysis is applied to find the correlation of all dependent and independent variables. Student's t-test is used for continuous variables between two set of data. Bland-Altman analysis (GraphPad Prism 6) is used to determine inter-observer and intra-observer variability.

3. Results and Discussion

3.1. LV-RV Comparison

At resting state, the comparison of each subject's LV and RV stroke volumes is not different, as expected under physiological conditions, where the stroke volumes of the RV and LV are equal assuming that all valves are in capable condition. Furthermore, we found a close correlation between LVSV and RVSV (r=0.717, p<0.0001) as shown in Figure 5A. Bland-Altman analysis test the degree of measurement agreement between RV and LV SV that shows a mean difference of 3.39 ml with close limits of agreement (± 6.79 ml, representing ±2 SD) as shown in Figure 5B.

Here, this is our main validation tool to confirm the suitability of our volume calculation method. It can be inferred that whether a patient is suffering from CVD. This also validates that the values we got from using the right ventricle systolic pressure to compute for the PA, PWV and AC are conclusive.

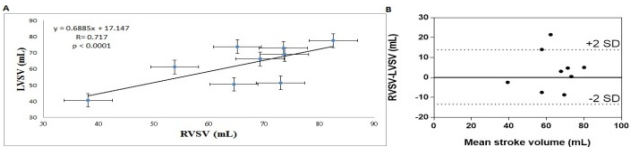

Figure 5. The result of (A) regression analysis of the comparison between RV and LV stroke volumes as assessed by CT imaging, and (B) Bland-Altman analysis for the evaluation of the agreement between RVSV and LVSV measurements. The average of RV and LV SV for each patient (*x*-axis) and the difference between RV and LV SV for each patient studied (*y*-axis)

3.2. Image Segmentation

The result of the seeded region growing algorithm is shown in Figure 6. A representative slice is the segmentation of the left ventricle (Figure 6A) while the segmentation of the right ventricle Figure 6B is shown as another representative slice. For each time series, we seeded 121±10 frames which collectively constitute to 1162±109 image frames processed for each patient's RV and LV volume determination. The images are over segmented with the seeded region growing algorithm. This over segmentation is responsible to the algorithm's pixel-order dependency, which means that all varying pixels within the defined range of intensity similarity, it is considered as part of the region of interest.

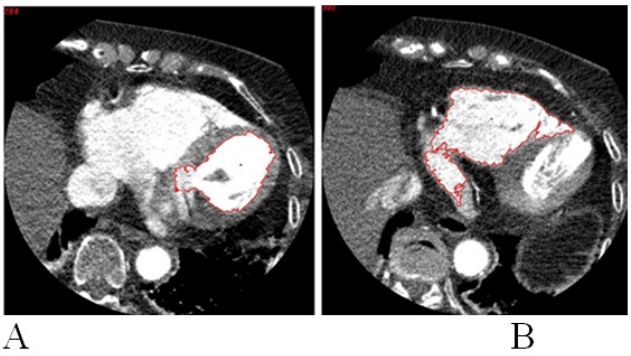

Figure 6. The result of seeded region growing algorithm is showing endocardial boundary of (A) The left ventricle and (B) The right ventricle with over segmentations

These over segmentations are overcomed by using the snake algorithm. We have kept our ROIs with the manual traced line to all the endocardial outlines to achieve good image segmentations as shown in Figure 7

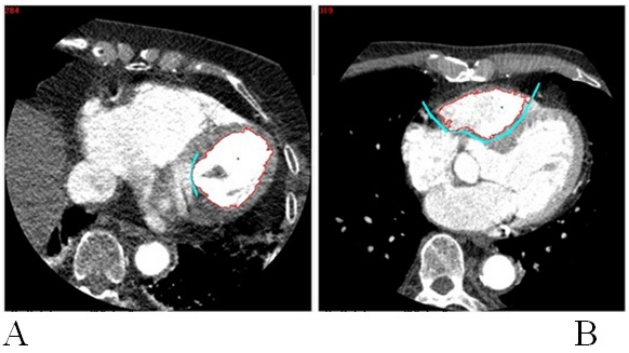

Figure 7. The result of the snake algorithm is showing endocardial boundary of (A) left ventricle and (B) right ventricle without over segmentation

These over segmentations are overcome by using the snake algorithm. We have kept our ROIs with the manual traced line to all the endocardial outlines to achieve good image segmentations as shown in Figure 7. The pulmonary artery image segmentation is shown as representative slice (Figure 8A). In this study, we have focused on determining the volume of the main pulmonary artery because of two reasons: (1) it is Geometrically stable for our mathematical models to work, and (2) our RVSP data for arterial compliance determination is only suited for main PA volume calculation. Hence, to determine the endocardial boundary of the PA, we first reconstructed the 3D model of the image (Figure 8B) to eliminate the left and right pulmonary artery as well as some unnecessary pulmonary veins using the tangent plane slicer. For the best volume calculation, each image plane has to perpendicular to the direction line of calculation. Therefore, the image was then resample three dimensionally, which is shown the right central axis position in six slices up and six slices down (Figure 8C). For each time series, we seeded 19±2 frames, which collectively constitute to 201±9 image frames processed for each patient's PA volume determination.

After all the ROIs image frames have been processed, a three-dimensional resample image of the entire heart is built, which shows the distinct endocardial boundaries of the LV, RV, and PA (Figure 9).

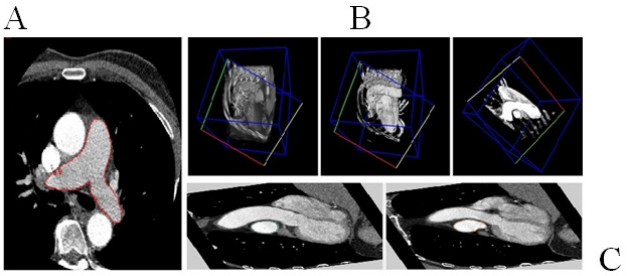

Figure 8. Segmentation of PA: (A) SRG segmentation result of the whole pulmonary artery, (B) 3D reconstruction and main PA determination, and (C) reconstructed 3D model were shown mainly using in PA volume extraction.

After all the ROIs image frames have been processed, a three-dimensional resampled image of the entire heart is built, which shows the distinct endocardial boundaries of the LV, RV, and PA (Figure 9)

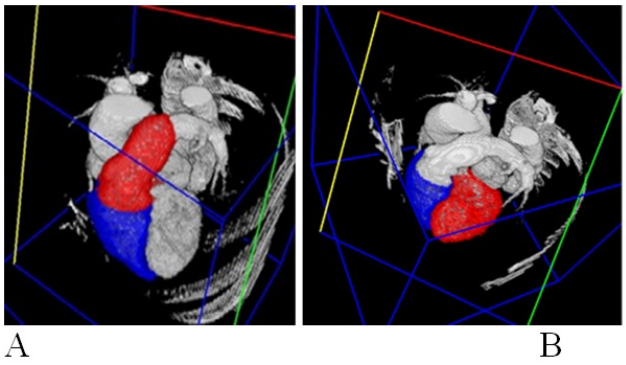

Figure 9. 3D resampled image of the heart is showing (A) the main pulmonary in red and right ventricle in blue and (B) the left ventricle in red and right ventricle in blue

3.3. Compliance

Comparison of right ventricular compliance versus PWV and pulmonary arterial compliance versus PWV has showed negative correlation r=-0.771, p=0.006 and r=-0.746, p<0.0001, as shown (Figure 10). This negative correlation results from the reduction in the compliance value that leads to a significant increase in pulse wave speed, and consequently arrival of reflected pulse waves during early systole, further amplify peak systolic pressure as well as pulse pressure.

The correlation of RV and PA vary between our two groups of patients. Regression analysis shows that the correlation between the RV and PA compliance of SR & AF patients are low (r=0.464, p<0.0001) (Figure 11A). On the contrary, the RV and PA compliance of patients with SR into AF , have positive correlation (r=0.962, p=0.02) (Figure 11B). Also, Table 1 shows that the patients vital information of arterial and ventricular compliance between the two groups of patients.

Pulmonary artery embolous can greatly affect the compliance of the pulmonary artery as shown (Figure 11A). For patients suffering from stroke into atrial fibrillation the integrity of the ventricles and pulmonary artery would remain intact [16]. Hence, the compliance would not be affected yet as shown on (Figure 11B).

3.4. Pulse Wave Velocity (PWV)

The comparison of pulse wave propagation plots for our nine subjects is shown in Figure 12. From processing large amounts of data, it is shown that the steepest slopes in each patient's pulse wave propagation plot are the least influenced by wave deformations and wave reflections. The steepest slope therefore defines the impulse representation of the pulse wave. Thus, by determining the first slice to intersect with the representative impulse (steepest slope), we are able to identify the starting point of the impulse itself and ultimately calculate the pulse wave velocity for each patient.

The results of the 64-MDCT is determined measurements of RV, LV, and PA volumes for the population (Table 1). The mean ± SD of the entire study group is 0.10±0.046 ml/mmHg for the pulmonary arterial compliance and 0.18±0.061 m/s for PWV.

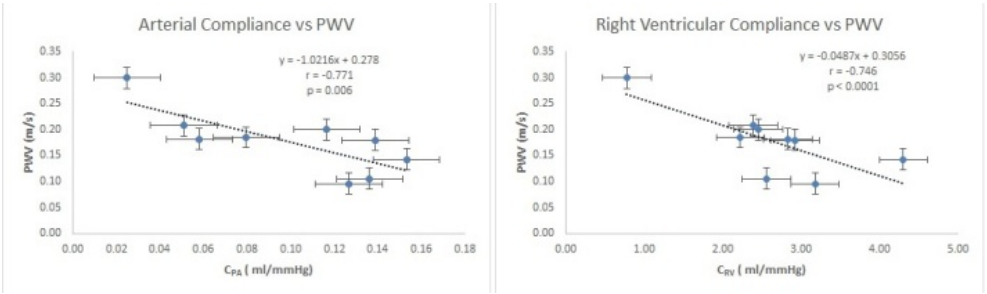

Figure 10. Result of the regression analysis of the comparison between (A) pulmonary arterial compliance and pulse wave velocity, and (B) between right ventricular compliance and pulse wave velocity

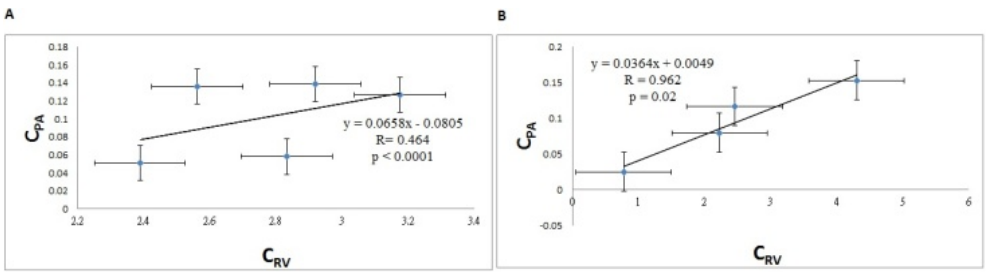

Figure 11. Right ventricular compliance and pulmonary compliance of patients with (A) AF and SR and (B) SR into AF

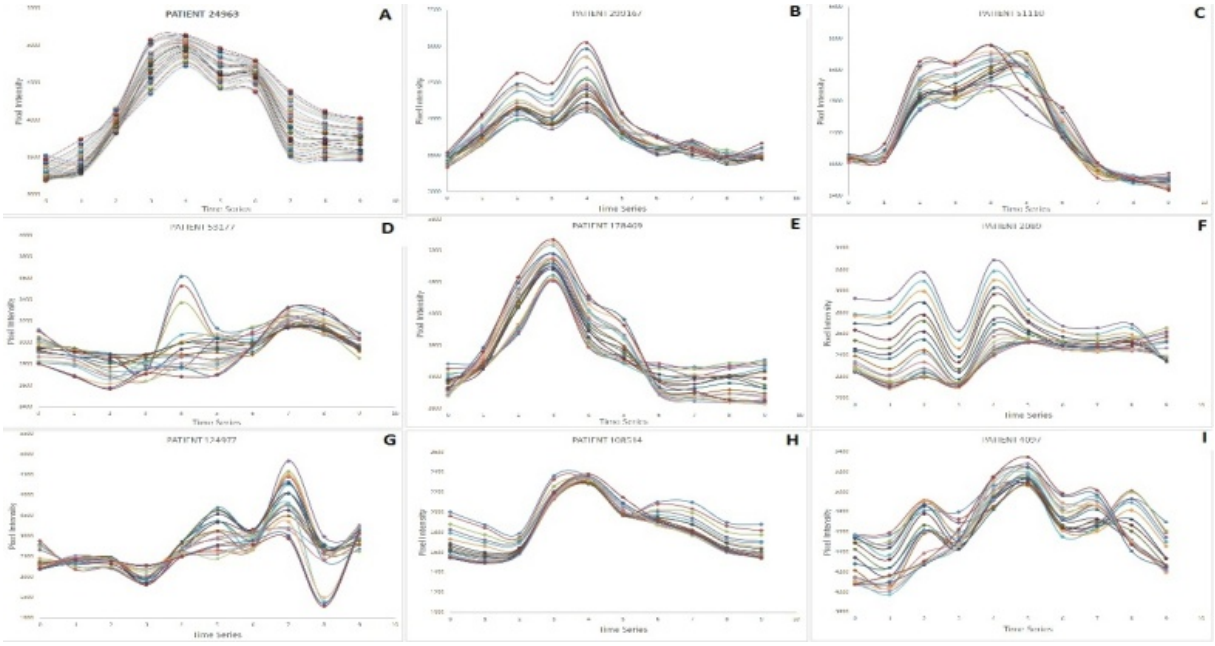

Figure 12. Pulse wave propagation (PWP) plot for our nine patients are showing the time series (x-axis) vs the pixel intensity (y-axis)

Table 1. Measurement results of entire study group

Subjects	CVD	Age	Heart Rate, beats/min	SV (mL)		PA,ΔV(ml)	C_{RV} ΔV/ΔP(ml/mmHg)	C_{PA} ΔV/ΔP(ml/mmHg)	PWV(Δd/Δt) m/s
				LV	RV				
1	SR into AF	78	66.75	68.96	73.71	3.50	2.46	0.12	0.20
2	SR into AF	72	56.00	50.46	64.53	2.30	4.30	0.15	0.14
3	SR into AF	69	56.00	72.99	73.49	2.63	2.23	0.08	0.18
4	SR into AF	86	74.00	40.49	38.10	1.23	0.78	0.03	0.30
5	AF & SR	64	70.20	61.20	53.78	2.86	2.56	0.14	0.11
6	AF & SR	42	60.60	73.83	65.18	1.34	2.83	0.06	0.18
7	AF & SR	82	53.00	77.51	82.56	3.29	3.18	0.13	0.10
8	AF & SR	76	63.00	51.44	72.97	3.47	2.92	0.14	0.18
9	AF & SR	67	63.00	66.15	69.25	1.48	2.39	0.05	0.21
Mean ± SD		70.67±12.89	62.50±6.97	62.56±12.61	65.95±13.13	2.46±0.92	2.63±0.93	0.10±0.046	0.18±0.061

Values are mean ± SD; n = 9 total number of eligible patients (LV - left ventricle, RV - right ventricle, PA - pulmonary artery, C_{RV} - right ventricle compliance, C_{PA} - pulmonary artery compliance, PWV - pulse wave velocity).

The results of the comparison in terms of the mean ± standard deviation of the calculated arterial compliance and pulse wave velocity between our two groups of patients (Table 2). The PWV of patients with stroke into atrial fibrillation (0.21±0.0665 m/s) is greater than those with both stroke and atrial fibrillation (0.15±0.0502 m/s). Our result agreed with the physiological fact that patients suffering from atrial fibrillation would have excessively high rate of cardiac contraction caused by disorder in the heart's electrical impulses [9].

Table 2. Comparison of arterial compliance, ventricular compliance and pulse wave velocity between two groups of patients

Cardiovascular Disease	C_{PA} (mean ± sd)	C_{RV} (mean ± sd)	PWV (mean ± sd)
SR into AF	0.09 ± 0.0547 ml/mmHg	2.44±1.447 ml/mmHg	0.21±0.0665 m/s
AF&SR	0.10 ± 0.0438 ml/mmHg	2.78±0.308 ml/mmHg	0.15±0.0502 m/s

3.5. Reproducibility and Variability

We calculated intra and inter observer coefficient of variation for C_{PA} is 10.79%, 15.55%, 10.15% and 14.00% for PWV. Regression analysis showed good intra- and inter-observer correlation between measurements: r=0.975, r=0.951 for C_{PA} , r=0.989, r=0.902 for PWV respectively. Bland-Altman analysis, with 95% limit of agreement, showed intra- and inter-observer differences equal to 0.008 ml/mmHg (-0.0124-0.0276 ml/mmHg) and 0.008 ml/mmHg (-0.0206-0.03658 ml/mmHg) for C_{PA} and 0.006 m/s (-0.0228-0.0347 m/s) and -0.0115 m/s (-0.0536-0.0305 m/s) for PWV (Figure 13, Figure 14).

We noted good reproducibility in image analysis as reflected by the coefficient of variation calculation of 10.79% and 10.15% for intra-observer calculations, 15.44% and 14.00% for inter-observer calculations, and low variability on the Bland-Altman analysis. The C_{PA} and PWV calculated by two observers showed correlation which is r=0.975 and r=0.951, respectively. From the two observers, one has good experience in off-line cardiac CT image processing while the other one did not have previous experience in this field, but received training on medical image processing from Chung Yuan Christian University Department of Biomedical Engineering. This reaffirms that the proposed methodology is highly reproducible and can be done by anyone with minimum amount of training, thus making the entire process less expensive.

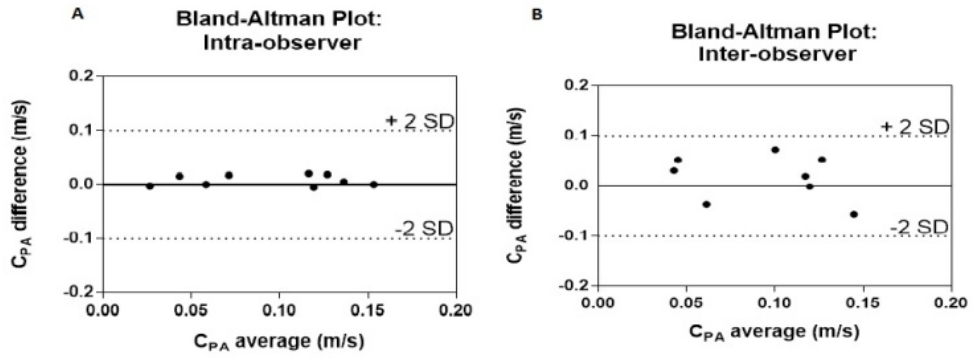

Figure 13. Intra- and inter-observer Bland-Altman analyses for pulmonary arterial compliance. Mean (95% limits of agreement) intra- and inter-observer differences were 0.008 ml/mmHg (-0.0124-0.0276 ml/mmHg) and 0.008 ml/mmHg (-0.0206-0.03658 ml/mmHg), respectively

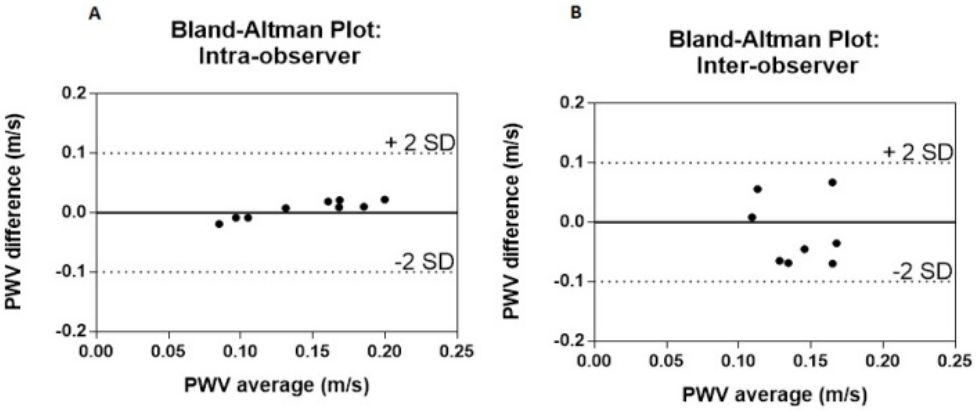

Figure 14. Intra- and inter-observer Bland-Altman analyses for pulse wave velocity. Mean (95% limits of agreement) intra- and inter-observer differences were 0.006 m/s (-0.0228-0.0347 m/s) and -0.0115 m/s (-0.0536-0.0305 m/s) for PWV, respectively

Our method should be applicable for calculating PWV and compliance for any other vessel where CT imaging processing approach is commonly used. The segmentation and volume calculation algorithms could also be easily modified to four-dimensional (4-D) data analysis.

Compared to other methods in calculating pulse wave velocity and compliance, our method exhibits the general advantages and disadvantages of the flow-area (QA) [17] and cross-correlation (XC) methods [18].

The proposed method is performed using data sets, which validates the accuracy of the results obtained. PWV and AC are also correlated using parameters measured from the right ventricle done by National Yang-Ming University Hospital prior to CT image acquisition. This research is the first study to propose such methodology which is less expensive. Thus making medical diagnosis of various cardiovascular diseases is affordable and readily available.

In this study, we developed a new methodology of pulse wave velocity (PWV) and compliance calculation from three-dimensional cardiac CT images. The CT images are acquired from ten-timed-series-ECG-gated 64-row Multidector Computed Tomography. We designed an effective integration of segmentation, correction and volume estimation algorithms as a basis for PWV and compliance determination using parameters from right ventricle volume calculation.

We also used a technique to determine the start of the impulse from the impulse propagation plot by using the first slice to intersect the steepest slope in each of the pulse wave plot.

The main validation of the tool is the calculation of the stroke volume of both the LV and the RV, which must be equal assuming all valves are competent. The proposed method is found to be highly reproducible with low variation by determining the Bland-Altman analysis intra- and inter-observer variability. Therefore, the derived methodology to calculate PWV from 3D CT cardiac images could be used as an index in evaluation of arterial stiffness.

Acknowledgments

The study is supported by Ministry of Science and Technology, Taiwan, Republic of China, under grant NSC-102-2221-E-033-004 and NSC-101-2221-E-033-003. João Manuel R.S. Tavares gratefully acknowledges the funding of Project NORTE-01-0145-FEDER-000022 - SciTech - Science and Technology for Competitive and Sustainable Industries, by "Programa Operacional Regional do Norte" (NORTE2020), through "Fundo Europeu de Desenvolvimento Regional" (FEDER).

References

[1] Babin, D., Devos, D., Pizurica, A., Westenberg, J. et al. Robust segmentation methods with application to aortic pulse wave velocity calculation. Computerized Medical Imaging and Graphics, 2013, 179-189.

[2] Cabrera, S.R.M., Lucas, C.T., Ruiz, S.G. et al. Relation between atrial fibrillation and pulse wave velocity in hypertensive patients. The Journal of Clinical Hypertension, 2012, 14 Suppl 1:151.

[3] Fielden, S.W., Fornwalt B.K., Jerosch-Herold, M., et al. A new method for the determination of aortic pulse wave velocity using cross-correlation on 2D PCMR velocity data. J Magn Reson Imaging, 2008, 27, 1382-1387.

[4] Horvath, I., Lenkey, Z., Alessandri N., Tufano, F., Kis, P., et al. Invasive validation of a new oscillometric device (arteriography) for measuring augmentation index, central blood pressure and aortic pulse wave velocity. Journal of Hypertension; 2010,28(10): 2068-75.

[5] Gasecki, D., Rojek, A., Kwarciany, M., Kowalczyk, K., et al. Pulse wave velocity is associated with early clinical outcome after ischemic stroke. Atherosclerosis, 2012, 348-352.

[6] Ohnesorge, B.M., Becker, C.R., et al. Multi-slice CT in Cardiac Imaging. New York, NY: Springer-Verlag Berlin Heidelberg, 2002.

[7] Graham, R.N.J., Perriss, R.W., Scarsbook, A.F. DICOM demystified: A review of digital file formats and their use in radiological practice. Clinical Radiology, 2005,60, 1133- 1140.

[8] Adams, R., Bischof, Leanne. Seeded region growing. IEEE Transactions on Pattern Analysis and Machine Intelligence, 1994, Vol. 16, 641-647.

[9] Chang, S.L., Tai, C.T., Lin, Y.J., et al. The role of left atrial muscular bundles in catheter ablation of atrial fibrillation. J Am Coll Cardiol , 2007, 50: 964-973.

[10] Tsao, H.M., Hu, W.C., Wu, M.H., et al. Quantitative analysis of quantity and distribution of epicardial adipose tissue surrounding the left atrium in patients with atrial fibrillation and effect of recurrence after ablation. Am J Cardiol, 2011, 107: 1498-1503.

[11] Ohnesorge, B.M., Becker, C.R., Flohr, T.G., Reiser, M.F. Multi-slice CT in Cardiac Imaging. New York, NY: Springer-Verlag Berlin Heidelberg, 2002.

[12] Tsao, H.M., Hu, W.C., Wu, M.H., Tai, C.T., et al. The impact of catheter ablation on the dynamic function of the left atrium in patients with atrial fibrillation: insights from four-dimensional computed tomographic images. J Cardiovasc Electrophysiol. 2010, 21: 270-277.

[13] Gatehouse, P.D., Keegan J., Crowe, L.A., et al. Applications of phase-contrast flow and velocity imaging in cardiovascular MRI. European Radiology, 2005, 15(10); 2172-84.

[14] Ibrahim, E.S., Johnson, K., Miller A., White, R. Measuring aortic pulse wave velocity using high-field cardiovascular magnetic resonance: comparison of techniques. Journal of Cardiovascular Magnetic Resonance; 2010, 12 (1), 26-26.

[15] Pannier, B.M., Avolio, A.P., et al. Methods and devices for measuring arterial compliance in humans. American Journal of Hypertension, 2002, 15: 743-753.

[16] Canadas, V., Vilacosta, I., Luaces, M., Bustos, A. et al. Thrombosis in an apparently normal thoracic aorta and arterial embolism. Revista Espanola de Cardiologia. 2008,Vol. 6, 196-200.

[17] Spencer, M.P., Denison, A.B. Jr..Pulsatile blood flow in the vascular system. Handbook of Physiology. Circulation. II Am. Physiol. SocWashington, DC, 1963, chapt. 25, p.842.

[18] Cullington, D., Goode, K.M., Zhang, J., et al. Is heart rate important for patients with heart failure in atrial fibrillation? JACC: heart Failure, 2014, Vol. 2, 213-220.

[19] Halliburton, S., Arbab-Zadeh, A., Dey, et al. State-of-the-art in CT hardware and scan modes for cardiovascular CT. Journal of Cardiovascular Computed Tomography, 2012, 6, 154-163.

[20] Kass, M., Witkin A., Terzopoulos, D. Snakes: Active Contour Models. International Journal of Computer Vision, 1998, 323-331.

[21] Lim, H.S., and Lip, G.Y.H. Arterial stiffness: beyond pulse wave velocity and its measurement. Journal of Human Hypertension, 2008, 656-658.

[22] Parisi, A.F., Moynihan, P.F., Feldman, C.L., Folland, E.D. Approacehs to determination of left ventricular volume ejection fraction by real-time twodimensional echochardiography. Clin. Cardiol, 1979,2, 257-263.

[23] Vulliemoz, S., Stergiopulos, N., Meuli, R. Estimation of local aortic elastic properties with MRI. Magn Reson Med., 2002, 47, 649-654.